

Excellence in Chemistry Research

Announcing our new flagship journal

- Gold Open Access
- Publishing charges waived
- Preprints welcome
- Edited by active scientists



Meet the Editors of *ChemistryEurope*



Luisa De Cola

Università degli Studi
di Milano Statale, Italy



Ive Hermans

University of
Wisconsin-Madison, USA



Ken Tanaka

Tokyo Institute of
Technology, Japan

“The Effects of Silver Nanoparticle Shape on Protein Adsorption and Neural Stem Cell Viability”

Murali Kumarasamy,^{*[a, b]} Ngoc Tran,^[c, e] Javier Patarroyo,^[c] Sushmita Mishra,^[a] Marco Monopoli,^[d] Emilia Madarasz,^[b] and Victor Puentes^[c, f]

Silver nanoparticles (AgNPs) are important and widely used as antimicrobials and nanodrug carriers. The increased use of AgNPs in consumer products has raised concerns about nano-safety; for instance, AgNPs may be inhaled and translocated to the brain via olfactory neural stem cells/progenitors. While the biological effects of nanoparticle size have been widely investigated, there are little data on the effects of particle shape on cellular phenotype. Therefore, here we investigated the interactions between AgNP spheres, rods, cubes, and triangles and human plasma proteins as well as their effects on the viability of NE-4C neural stem cells. Nanoparticles were synthesized by wet chemistry methods and characterized by

UV-vis spectroscopy, dynamic light scattering, zeta potential measurement, transmission electron microscopy, nanoparticle tracking analysis, and differential centrifugal sedimentation. NE-4C cell viability was assessed using the MTT reduction assay, and the cellular uptake of differently shaped nanoparticles was monitored by electron microscopy. All 50 nm (in at least one dimension) AgNPs exerted toxic effects, with rods and cubes displaying greater toxicity than spheres and triangles. These cellular and physicochemical results indicate that edges on the AgNPs increase toxicity, presumably due to enhanced ion dissolution from the edges.

Introduction

Silver nanoparticles (AgNPs) are widely used in a variety of commercial applications including electronics, paints, clothing, food, cosmetics, and medical devices due to their desirable catalytic, optic, magnetic, and antibacterial properties. According to the Woodrow Wilson database, about 50% of all consumer products are thought to contain engineered nanosilver.^[1] As a consequence of this widespread use, humans are potentially exposed to AgNPs through the dermal, oral, or

inhalation routes. AgNPs can be inhaled during their manufacture or their subsequent use, such as when used as aerosol disinfectants or as over-the-counter homeopathic sprays for the treatment of respiratory infections.^[2] By virtue of their small size, AgNPs can easily penetrate into the lower respiratory tract, which, through its specialization for gaseous exchange with the circulation, possesses an immense surface area for their deposition and systemic transport.

However, AgNPs have also been shown to have effects on the central nervous system.^[3] They can enter the nasal epithelium and translocate to the brain region via the olfactory epithelium (OE), and olfactory bulb (OB) which directly connects the brain tissues.^[2d,3-4] In particular, animal modeling has shown that some nanomaterials (NMs) can translocate to the brain to affect its nerve function.^[5] NMs, viruses, and other molecules can bypass the blood-brain barrier (BBB) and be transported from the nasal epithelium to the OE and OB in the forebrain^[4a,5a,6] via three potential pathways: a) transcellular transport across sustentacular cells of the OE; b) paracellular transport through junctions in the OE; or c) intracellular transport through axonal movement via olfactory nerve fascicles (ONFs) to the synaptic junctions within the OB.^[6] Nanoparticle translocation along ONFs and accumulation in the OB have been particularly well studied.^[2d,4a,7] Mechanistically, AgNPs have been shown to dysregulate a number of different cell types and signaling pathways both *in vitro* and *in vivo*. AgNPs introduced into the systemic circulation can induce BBB dysfunction, astrocyte swelling, and neuronal degeneration.^[8] AgNPs have been reported to block the vascular endothelial growth factor (VEGF)-induced proliferation and migration of bovine retinal endothelial cells (BRECs) and induce apoptosis.^[9] AgNPs have been shown to increase the membrane permeability of primary rat brain endothelial cells by activating

[a] Dr. M. Kumarasamy, S. Mishra

Department of Biotechnology, National Institute of Pharmaceutical Education and Research (NIPER), Hajipur (Dept. of Pharmaceuticals, Ministry of Chemicals & Fertilizers, Govt. of India), Export Promotion Industrial Park (EPIP), Industrial Area, Hajipur - 844 102, District: Vaishali, State Bihar, India
E-mail: drmuralinano@gmail.com

Homepage: <http://www.niperhajipur.ac.in>

[b] Dr. M. Kumarasamy, Prof. Dr. E. Madarasz

Laboratory of Cellular and Developmental Neurobiology, Institute of Experimental Medicine of the Hungarian Academy of Sciences, Budapest, Hungary

[c] Dr. N. Tran, Dr. J. Patarroyo, Prof. Dr. V. Puentes

Catalan Institute of Nanoscience and Nanotechnology (ICN2), CSIC and BIST, 08193 Barcelona, Spain

[d] Dr. M. Monopoli

Centre for BioNano Interactions, School of Chemistry and Chemical Biology and Conway Institute for Biomolecular and Biomedical Research, University College Dublin, Belfield, Dublin 4, Ireland

[e] Dr. N. Tran

Department of Scientific Management, Dong A University, Da Nang, Vietnam

[f] Prof. Dr. V. Puentes

Institució Catalana de Recerca i Estudis Avançats (ICREA), 08010 Barcelona, Spain

 Supporting information for this article is available on the WWW under <https://doi.org/10.1002/slct.202201917>

proinflammatory mediators.^[10] 20 nm AgNPs were found to activate rat lung epithelial (RLE) and rat aortic endothelial (RAEC) cells in an interleukin-6 (IL-6)-dependent manner.^[11] Furthermore, AgNPs but not Ag⁺ ions have been shown to induce inflammatory signaling pathways.^[12] Clathrin-mediated endocytotic uptake and cytoplasmic and nuclear accumulation of AgNPs have been observed in U251 human glioblastoma cells,^[13] and AgNPs have been shown to accumulate in primary astrocytes in a concentration-dependent manner.^[14] 20 and 80 nm AgNPs affected the growth of human embryonic neural precursor cells,^[15] and all retinal neuronal layers took up the particles and displayed neural damage.^[15] Finally, AgNPs have been shown to affect neurite outgrowth and reduce the viability of premature neurons and glial cells.^[16] Recent studies have also demonstrated that the geometries of NPs impact protein corona formation,^[17] circulation time, cellular uptake, and bio-distribution.^[18] In the last few years, we conducted systematic *in vitro* 2-dimensional^[19] and 3-dimensional (brain organoids and spheroids)^[20] studies to evaluate cellular neurosafety and neural uptake of well-characterized polymeric, metallic (Ag and Au) and ceramic NPs. Among various physicochemical properties known to influence biological activities, in this study we focused on the different shape of Ag NPs. There is a growing body of evidence that AgNPs can have adverse effects on the central nervous system. However, there have been few studies of the effects of different shapes of AgNP on neural cell function. Since the growth, shape, and size of AgNPs can easily be modified using polyvinylpyrrolidone (PVP) as a structure-directing polymer,^[21] here we investigated the synthesis and cellular effects of different shapes of PVP-coated AgNP on NE-4C neural stem cells.

Results

Synthesis and physicochemical characterization of differently shaped AgNPs

Cubic, and rod-shaped AgNPs were synthesized using the polyol process,^[22] with polyvinylpyrrolidone (PVP) as the protecting agent and ethylene glycol (EG) as both the reducing agent and solvent. In this synthesis, the reaction temperatures and times as well as the concentration of protective agent are the key parameters controlling the size and geometries of the metal particles.^[23] The sphere diameters and edge lengths of nanocubes and triangles, respectively, were 35–55 nm, while the thickness of triangular platelets was ~5 nm and the lengths of rods 40–70 nm in cross-sectional diameter reached several micrometers. The different geometries of AgNPs were characterized by transmission electron microscopy (TEM) and UV-vis spectroscopy,^[24] with the spherical AgNPs also characterized by nanoparticle tracking analysis (NTA) and differential centrifugal sedimentation (DCS). UV-vis spectroscopy exploits the surface plasmon resonance (SPR) of metal nanoparticles to reflect the abundance of edges and sharp points in the particles.^[24]

Spherical AgNPs were produced at concentrations of 0.1 g/L or 1.5×10^{11} NPs/mL. Monodisperse suspensions were stabilized with either sodium citrate or PVP in the solvent. UV-vis

spectrum (Figure 1A) revealed the typical optical characteristics of a colloidal suspension of ~50 nm spherical AgNPs. The size distribution was determined by NTA (Figure 1B) and by TEM (Figure 1C), which indicated 47 ± 3 nm and 47 ± 7.8 nm particle sizes, respectively. The TEM images revealed spherical, mainly monodisperse particles (Figure 1C). Monodispersity was also confirmed by DCS (Figure 1D). The zeta-potential of the spherical AgNPs was -20 mV in PVP-stabilized suspensions.

Silver nanocubes were synthesized by reducing silver trifluoroacetate with EG in the presence of PVP. Thirty minutes after the addition of CF₃COOAg, Ag nanocubes with an edge length of 35–40 nm were obtained. UV-vis spectroscopy (Figure 2A) reveals a characteristic shoulder peak around 350 nm, indicating the presence of silver nanocubes,^[25] which was also confirmed by TEM (Figure 2B).

Silver nanotriangles were prepared by reducing an aqueous silver nitrate solution with NaBH₄ in the presence of trisodium citrate, PVP, and hydrogen peroxide (H₂O₂). PVP was used to improve the size distribution of the nanotriangles/plates. While the characteristic sharp shoulder peak around 330 nm can be caused by quadrupole resonance of silver nanotriangles,^[26] the long peak shifting towards longer wavelengths indicated the formation of nanotriangles/plates (Figure 2C), which was also confirmed by TEM (Figure 2D).

Silver nanorods were characterized by UV-vis spectroscopy (Figure 2E). The spectrum reflected the anisometric geometry of Ag nanorods, with a sharp absorbance at 350–390 nm, the optical fingerprint of Ag nanorods.^[27] The formation of silver nanorods was confirmed by TEM (Figure 2F), and the final concentration of freshly prepared Ag nanorods was 3.8×10^9 NPs/mL (1.08 g/L by ICP-MS).

Protein adsorption by AgNPs

We next studied the dispersion and protein corona formation with AgNPs incubated in human plasma at three concentrations [10, 80, and 100% (v/v in PBS)]. DCS measurements focusing on spherical NPs displayed that AgNP-protein complexes were monodisperse at all three human plasma concentrations (full corona, FC). The main plasma concentration peak shifted to the left, suggesting an increase in protein corona thickness (Figure 3A). This adsorption of proteins on the NP surface is typical for systems in which the protein density is lower than the NP density. As demonstrated in Figure 3A, at high plasma concentrations (from 80%), free plasma proteins sometimes aggregated. The Vroman effect^[28] predicts that the adsorption of blood serum proteins to inorganic surfaces is time-dependent: serum proteins with the highest mobility (or closest to the surface) arrive at the surface first and are gradually replaced by less motile proteins with a higher affinity for the surface; this process may take several hours. To study the effect of different geometries of silver NPs on protein corona formation (Figure 3B), we incubated the spherical, cubic, triangular, and rod-shaped AgNPs in human plasma for 1 and 24 h with continuous agitation. When AgNPs of different shapes were incubated with 100% human plasma, besides time dependency, the rate of protein adsorption was shape-

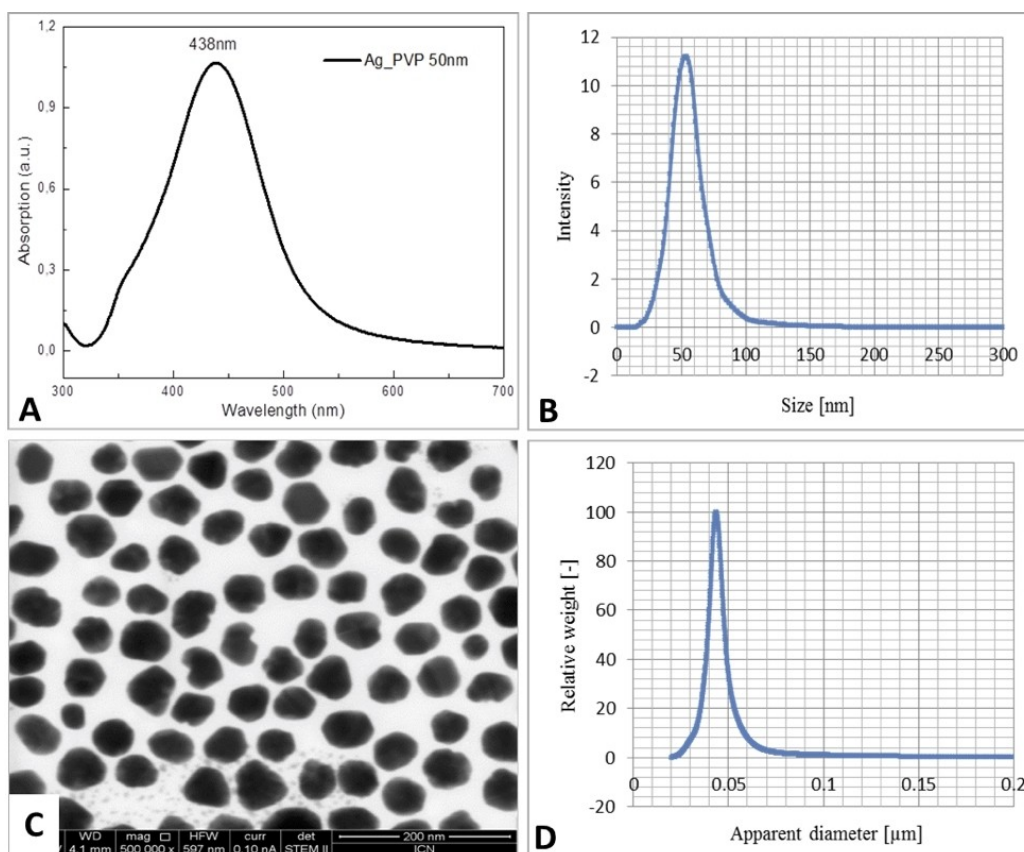


Figure 1. Characterization of spherical AgNPs by (A) UV-vis spectroscopy, (B) NTA, (C) TEM, (D) DCS.

dependent. AgNP consumption and protein corona formation *in situ* revealed that AgNPs with angles and edges adsorbed more proteins than those with a spherical shape after both short and long incubation times (Figure 3B). These results agree with a previous report that specific proteins such as lysozyme and α -chymotrypsin adsorbed more on metal nanorods compared to nanospheres.^[29]

The rod-shaped and triangular NPs, where the curvature is only one dimensional (1D), allow for greater protein density and adsorption, since increased lateral interactions on the relatively “flat” cylindrical surface facilitate protein adsorption compared to on spherical NPs.^[29]

Cellular responses to differently shaped AgNPs

AgNPs are known to be toxic to microbes and tissues, mainly due to the release of Ag⁺ ions.^[30] We therefore investigated the influence of particle shape on mammalian cellular toxicity. Differently shaped 50 nm AgNPs were incubated with NE-4 C embryonic neuroectodermal stem cells for 24 hours at increasing (1–100 mg/ml) concentrations, and the MTT metabolic assay was performed to assess cell viability. Metabolic activity (i.e., MTT reduction capacity) was reduced below 20% of control by Ag rods at 1 μg/mL and by cubes at 50 μg/mL concentrations (Figure 4A). Ag triangles exhibit mild (< 50%)

toxicity at 100 μg/ml, while Ag spheres were not toxic when compared to untreated controls.

AgNPs may also be toxic through the release of Ag ions, so NPs were dispersed (100 μg/mL) in cell culture medium and, after 24 hours of incubation, the particles were removed by centrifugation. Ag⁺ released by Ag NPs was measured by UV-Vis (Supplementary File). NE-4C cells were incubated with particle-free incubation solutions and cell viability assayed after 24 hours incubation. Cell viability was reduced by particle-free supernatants of Ag cubes and triangles but almost no toxicity was observed with the supernatants of spheres or rods (Figure 4A). In spherical NPs, all surface atoms have an approximately identical coordination number. In cubic, shaped NPs, however, the number of bonds of a surface atom will depend on its surface position: at the corners and edges, the coordination number will be smaller than on the planar surface areas. As less cohesive energy makes the atoms more reactive, the chemical surface activity of particles will depend on both, their size and shape. In our experiments, 40–50 nm cubic NPs with cornered/edged shapes will display higher surface activity than spherical particles of the same size.

Cellular uptake of AgNPs after 1 hour of incubation was investigated by electron microscopy (Figure 5). Ag rods resulted in mechanical damage to the cells. The local geometry of silver particles in contact with the cell membrane was important in determining how cells interacted with the micro-

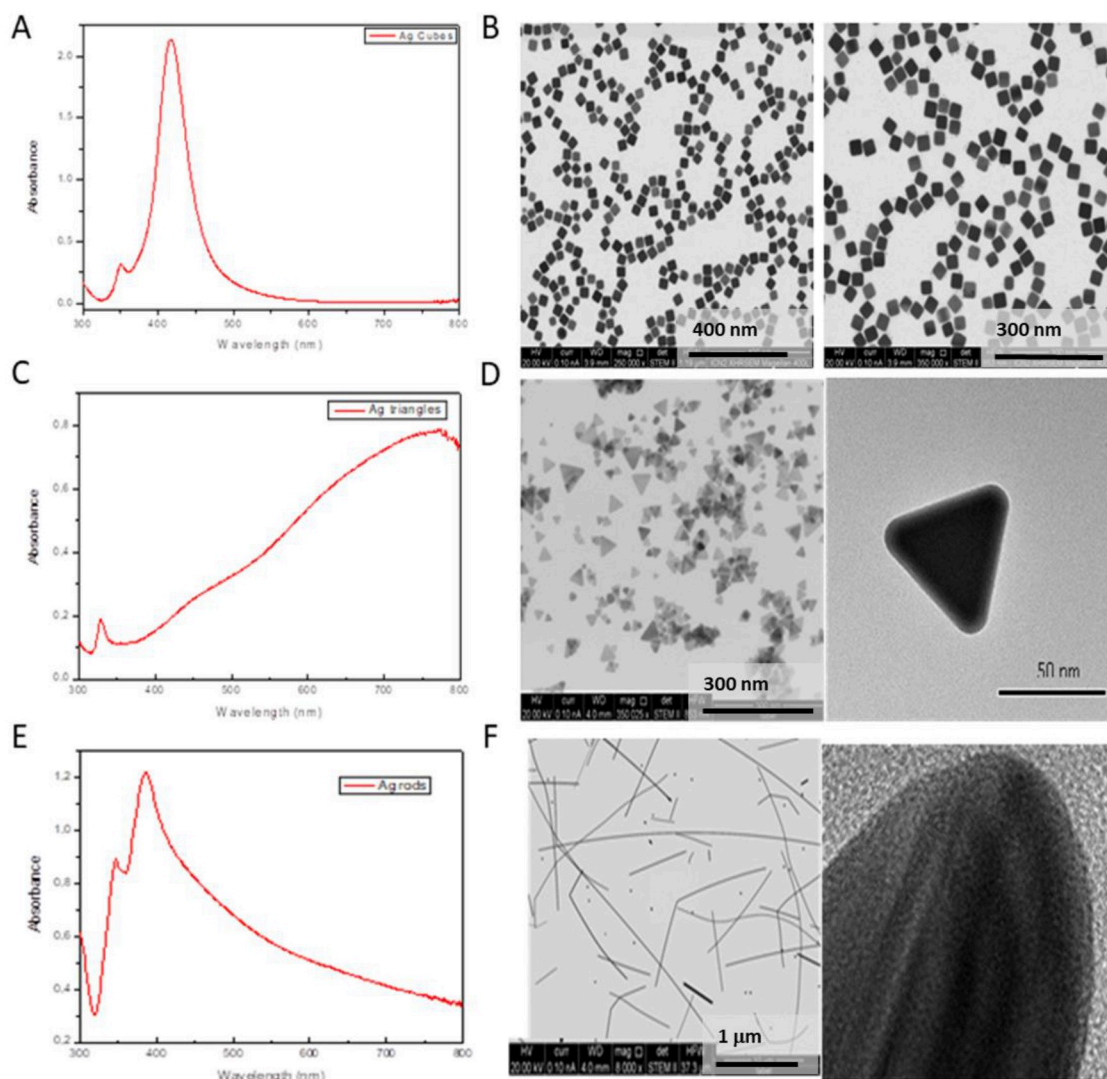


Figure 2. (A) UV-vis absorption spectrum of the aqueous solution of silver nanocubes with edge lengths of 35–45 nm. (B) TEM images of Ag nanocubes obtained by a standard polyol synthesis. (C) UV-vis absorption spectrum of the aqueous solution of Ag nanotriangles/platelets. (D) TEM and HR-TEM images of Ag nanotriangles/plates. By TEM, the synthesized product was triangular with edge lengths of 31.5 ± 11 nm and platelet thickness of 4.5 ± 0.9 nm. (E) UV-vis absorption spectrum of the aqueous solutions of silver nanorods. (F) TEM and HR-TEM images of Ag nanorods. TEM images show nanobars with lengths up to 5000 nm and widths of 60–80 nm, with aspect ratios between 60–80.

particles. For example, the sharp edges of rods in contact with the cell membrane allowed the particle to penetrate the cells. This may have been because the sharper contacting geometries made it easier for cells to recruit actin filaments to attach and engulf the objects compared to particles with a round surface. Overall, rod-like and sharp NP geometries made it more likely that they would adhere to and become internalized by the cell. Particles with different shapes in general, and rod-shaped NPs specifically, agglomerate, diffuse, and settle in cell culture medium. Therefore, increased cellular density is also a function of these factors, as it determines the rate of transport of NPs to cells in culture.^[31]

Electron microscopy failed to demonstrate accumulation of AgNPs in intracellular vesicles and revealed very few particles inside cells, perhaps due to low cellular penetration or the rapid dissolution of silver particles outside and inside cells.^[32]

In this work, we measured changes in the AgNPs with constant dissolution states after 4 and 24 hr by using ultraviolet-visible (UV/vis) absorbance spectrum measurements (Supplementary File). Importantly, this UV/vis does not require the separation of the AgNPs from dissolved Ag ions. Simultaneously, we compared the toxic effects of uncoated (0.001% w/v) standard citrate- and PVP-coated Ag-NPs in neural stem cells (Supplementary File). Our results showed that, not much variability of PVP-coated and uncoated AgNPs, at a concen-

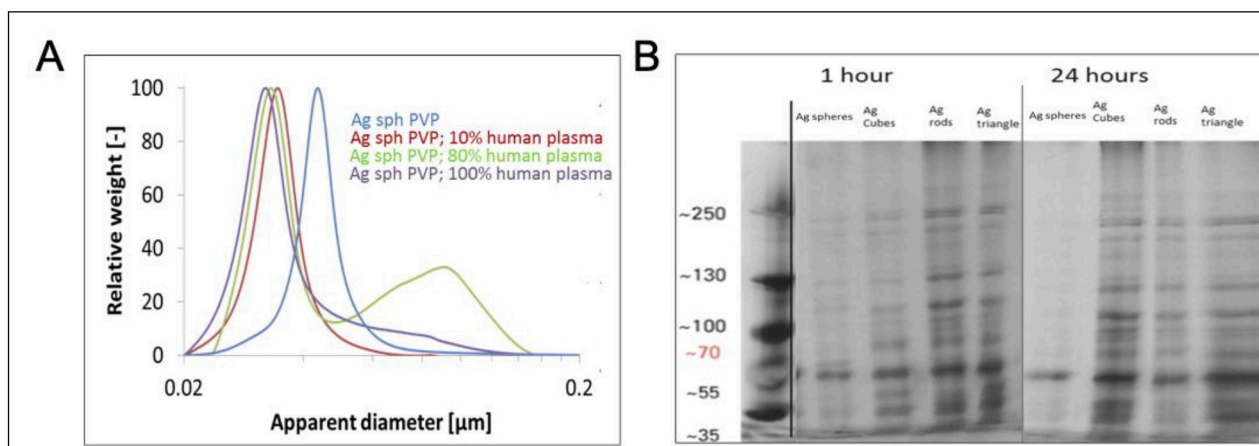


Figure 3. (A) DCS measurements of AgNP-corona complexes before and after incubation with plasma. (B) SDS-PAGE of the protein coronas of different forms of AgNPs incubated in 100% human plasma for 1 h and 24 h.

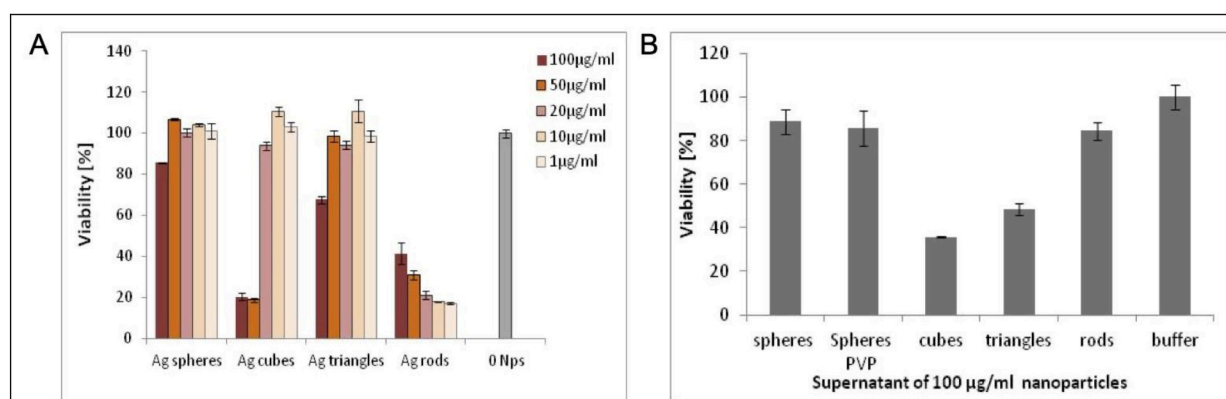


Figure 4. (A) Shape-dependent effects of AgNPs on the metabolic activity of NE-4 C neural stem cells (MTT assay). (B) The effects of particle-free supernatants of NP suspensions on the viability of NE-4 C cells. Spheres PVP: Ag spheres kept in PVP-containing buffer prior to dispersion in the culture medium.

tration of 0.001% w/v, on the other hand, Ag-rods produced extreme toxicity at this concentration.

DISCUSSION

Silver NPs (35–50 nm) exerted shape-dependent toxic effects on neural cells. Toxicity may be due to shape-dependent dissolution of Ag ions and the severe mechanical damage caused by rod-shaped NPs. Supporting this, previous studies have shown that NP shape affects the level of cellular toxicity.^[33] In a previous work, we demonstrated that, the low accumulation of 60 nm sized Ag NPs (60 ± 13 nm) in neurovascular blood-brain barrier (NV-BBB) organoids due to its dissolution outside and inside the brain microenvironment.^[20] There is therefore increasing data suggesting that the geometric properties of NPs mediate toxicity, but a more systematic approach would further advance our knowledge with

respect to exactly which shapes exert the most cytotoxic effects. Silver NPs are known to exert toxic effects on bacteria, fungi, and mammalian cells. AgNPs were variably toxic due to the variable dissolution of ions, with cubic and triangular NPs releasing more ions than spheres due to dissolution from the sharp edges. Our study shows, Ag rods exhibit very high toxicity and increased ion release (results not shown), perhaps due to their shape interacting with cellular membranes. Hence, shape can also influence the interaction between particles and cell membranes, and endocytosis or phagocytosis are influenced by edges and lines on particle surfaces^[33–34]

The shape of NPs has previously been shown to be important for mediating the toxic effects of nanomaterials.^[35] Indeed, our electron microscopy results indicated that Ag nanorods caused severe mechanical cellular injury rather than chemical toxicity. Although there were unexpectedly low number of particles inside NE-4 C neural stem cells after one

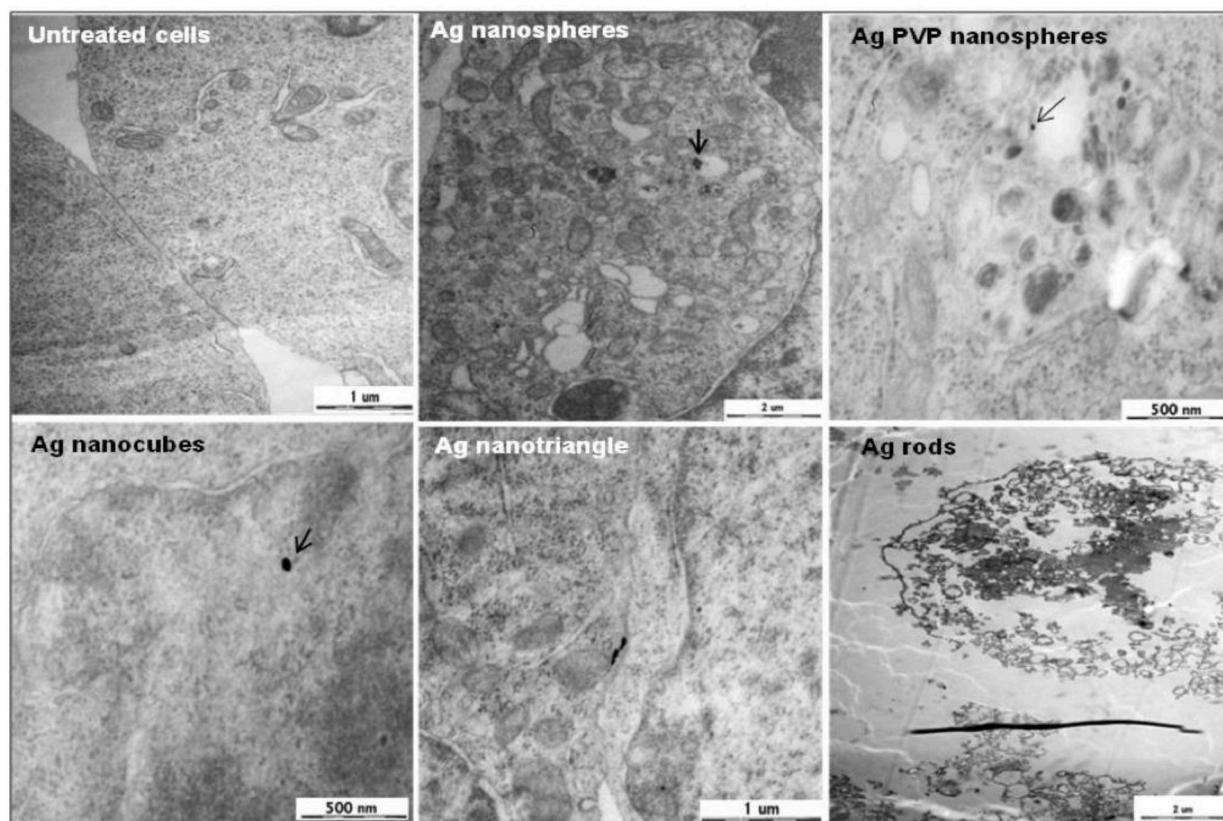


Figure 5. Spherical, cubical, or triangular AgNPs did not cause severe structural damage to NE-4 C cells after one hour of exposure. By contrast, NE-4 C cells were disrupted by Ag nanorods.

hour of exposure, the few nanorods that were present seemed to completely disrupt the cells.^[32] As all AgNPs produce silver ions with their associated kinetics and toxicity effects,^[36] their wide application as anti-bacterial medical and food packaging additives needs further consideration, particularly with respect to the optimal types and doses of AgNPs that minimize shape-dependent cytotoxicity.

Conclusion

In conclusion, while all shapes of AgNPs adsorbed large amounts of plasma proteins, the amount of adsorption was dependent on the shape. Similarly, cellular toxicity was shape-dependent: rods were highly toxic within an hour of exposure, and cubes and triangles were toxic at high concentrations after 24 hours. While rods presumably mediated their toxicity via mechanical damage, the shape might also result in the rapid release of Ag ions and indirect cytotoxicity. Our preliminary research urges nanomedicine community to focus on the toxicity of accidental AgNPs prior biomedical applications.

Experimental Section

Chemicals used

Ethylene glycol (anhydrous 99.8%, EG), silver trifluoroacetate (CF_3COOAg), polyvinylpyrrolidone (MW: 360,000), hydrochloric acid 37% (HCl), sodium hydrosulfide (NaHS), were purchased from Sigma-Aldrich. All chemicals were used as received without further purification.

Preparation of silver (Ag) NPs

50 nm PVP-coated AgNPs were synthesized according to Bastús and co-workers.^[37] Particularly, 1 mL of 0.5 M sodium citrate and 1 mL of 25 mM tannic acid were mixed with 97 mL H_2O in a three-neck round-bottomed flask. The mixture was heated to boiling with vigorous stirring followed by fast injection of 1 mL 50 mM AgNO_3 . NP growth was achieved by consecutive addition of 50 mM AgNO_3 (1 mL per addition). After each injection, the solution was kept under reflux to complete the reaction for 30 min. 50 nm spherical AgNPs were obtained at the 10th injection. The as-prepared NPs were centrifuged at 8000×g for 15 min prior to conjugation with PVP.

Conjugation of silver nanoparticles with polyvinylpyrrolidone

Synthesized AgNPs (~ 50 nm, 7.5×10^{11} NPs/mL) were redispersed in a fresh solution of 5 mM polyvinylpyrrolidone (PVP, MW =

55 kDa) and vigorously stirred for 72 h. Then, the AgNPs were washed again to eliminate excess PVP.

Synthesis of PVP-caped Ag nanocubes

Silver nanocubes were synthesized by a modified polyol method^[25] briefly 15 mL of EG was added to a 100 mL round-bottomed flask, the flask was closed and then it was heated in a silicon oil bath at 150 °C. The reaction solution was continuously stirred using a magnetic stir bar. After 10 min, 180 µL of 3 mM NaHS solution in EG was added. After 2 minutes, 500 µL of 3 mM HCl solution in EG and 3.8 mL of 20 mg/mL poly (vinyl pyrrolidone) were added. Finally, after 3 min, 1.2 mL of 282 mM CF₃COOAg solution in EG was added. During the entire process, the flask was capped with a glass stopper except when adding reagents. After addition of CF₃COOAg, the transparent solution became a whitish color and then slightly yellow after 1 min, indicating the formation of Ag seeds and then nanocubes.

After 60 min, the reaction was stopped by placing the reaction flask in an ice-water bath. Resultant Ag nanocubes were purified by centrifugation (8000 g, 20 min) in order to remove the EG and the excess of poly (vinyl pyrrolidone), and further redispersed in water before sample characterization.

Synthesis of PVP-caped Ag nanotriangles

PVP-coated Ag nanotriangles were synthesized as in.^[38] A 24.04 mL aqueous solution containing AgNO₃ (0.05 M, 50 µL), trisodium citrate (75 mM, 0.5 mL), PVP (40 K, 17.5 mM, 0.1 mL), and hydrogen peroxide (H₂O₂; 30 wt%, 60 µL) was vigorously stirred at room temperature in air. Sodium borohydride (NaBH₄, 100 mM, 250 µL) was rapidly injected into this mixture to initiate the reduction. The solution gradually turned from light yellow to dark blue within 60 min.

Synthesis of PVP-caped Ag nanorods

Silver nanorods were prepared as previously described by Zhan et al^[39] the method remarks that the slow dropwise addition facilitated the formation of pentagonal twinned seeds, and the second rapid dropwise addition provided a sufficient silver source, which led to the rapid growth of silver nanowires which will retain the pentagonal twinned morphology. Briefly, 0.5 mL of FeCl₃ solution (0.6 mM, in EG) was added to 6 mL EG in a round-bottom flask and was heated to 150 °C. Then, 6 mL EG solution containing 0.052 M AgNO₃ and 0.067 M PVP (average molecular weight 360 kDa) was added. The reaction mixture was kept at 150 °C with stirring at 250 rpm until AgNO₃ was completely reduced (about 70–90 min).

To examine the yield and morphology of Ag nanorods, 1 mL of the resulting suspension was diluted with 8 mL acetone and 8 mL ethanol and centrifuged at 2000 rpm for 10 min twice. At every stage, the supernatant solution was measured with a UV spectrometer to predict the presence of AgNPs in the solution. All the synthesized AgNPs were washed several times with water and then stored at 2–8 °C and protected from light.

Transmission electron microscopy (TEM)

TEM images were obtained with a JEOL JEM 1010 (JEOL Ltd., Tokyo, Japan) and Phillips CM20 (Phillips, Amsterdam, Netherlands) at

200 keV using carbon grids (S162, Plano GmbH, Wetzlar, Germany). Carbon grids were dried at room temperature (RT), and the areas of the grid were observed at different magnifications. TEM pictures were computer analyzed *in situ* and the size distribution and average size of particles were determined.

Dynamic light scattering (DLS) and Z-potential measurement

NPs suspended in water, phosphate buffered saline (PBS), 10% fetal calf serum in PBS, and culture medium were characterized by dynamic light scattering (DLS) and by zeta-potential determination (Malvern Zetasizer Nano ZS90; Malvern, UK). Particles were sonicated for approximately 20 seconds before being dispersed in the appropriate dispersants. All DLS measurements were performed with a Malvern Zetasizer Nano ZS90 (Malvern) operating at a light source wavelength of 532 nm and a fixed scattering angle of 173° on 1 mL aliquots of the NP suspensions. Zeta-potential and DLS assays were performed at 25 °C and 37 °C and are presented as averages and standard deviations of the data obtained from 3 to 5 assays in each solution.

UV-visible spectrophotometry of PVP-caped AgNPs

UV-visible spectra of 1 mL aliquots of the NP suspensions were assayed with a Shimadzu UV-2400 spectrophotometer in the 300–800 nm wavelength range. This technique provides characteristic absorbance maxima for metallic NPs (due to their surface plasmon resonance), which changes with the size, morphology, and surface alterations of the NPs. UV-vis extinction spectra were taken at room temperature using a 1 cm optical path quartz cuvette by diluting sample solutions into 1 mL.

Nanoparticle tracking analyses (NTA)

Nanoparticle tracking analyses (NTA) were performed using a Nanosight LM10 (NanoSight Ltd., Salisbury, UK) equipped with a red laser (630 nm) and CCD camera. The samples were dispersed in milli-Q water, and the experiments were performed at 22 °C. The Brownian motion of the particles was analyzed on 60-second records by the NTA software.

Differential centrifugal sedimentation (DCS)

DCS experiments were performed with a disc centrifuge (Model DC 24000; CPS Instruments Europe, Oosterhout, The Netherlands). A gradient of 2%–8% sucrose equilibrated with spinning at 22,000 rpm for 30 min was established and calibrated by running standard polystyrene beads. After establishment of the gradient, 100 µL aliquots of particles dispersed in water were injected. Samples were spun for approximately 2 hours for Ag NPs and 5–10 min for spherical AgNPs. The position of particles in the gradient was analyzed with CPS software. The tallest peak (the most frequent size value) was regarded as the 'base' peak (100%), and all other particle size peaks were normalized against this base peak (relative size distribution).

Human blood proteins on spherical PVP capped Ag NPs

In situ protein coronas on spherical PVP capped Ag NPs were prepared by incubating 0.1 mg/mL NPs in 10%, 80%, and 100% human plasma solution (total protein content 34–47 mg/mL) at room temperature for 1 hour.

The human plasma was obtained from the Centre for BioNano Interactions (CBNI), School of Chemistry and Chemical Biology, University College Dublin, Dublin, Ireland. The blood donation procedure was approved by the Human Research Ethics committee at University College Dublin. The blood plasma was prepared following HUPO BBB SOP guidelines.^[40] In brief, after blood collection, the blood was mixed with 2 mM EDTA and centrifuged for ten minutes at 1300×g at 4 °C. Plasma from each donor was collected into 50 mL Falcon tubes and then centrifuged at 2400×g for 15 min at 4 °C. The supernatant was collected, aliquoted into 1 mL cryovials, and stored at –80 °C until use. Following this procedure, the plasma protein concentration was estimated to be 80 g/L. Before the experiments, the plasma sample was thawed at RT and centrifuged for 3 min at 16,200 RCF. After incubation with human plasma, the NP samples were directly injected into the DCS instrument without spinning down and washing.

NE-4C neuroectodermal stem cell culture

NE-4C neuroectodermal stem cells (ATTC CRL-2925^[41]) were cloned from primary brain cell cultures prepared from the fore- and midbrain vesicles of 9-day-old transgenic mouse embryos lacking functional p53 tumor suppressor protein. NE-4C neuroectodermal stem cells were maintained in poly-L-lysine-coated culture dishes in minimum essential medium (MEM; Sigma Aldrich, St. Louis, MO) supplemented with 4 mM glutamine and 10% fetal calf serum (FCS; Sigma Aldrich) (MEM-FCS).

Cell exposure to nanoparticles

For viability assays, the cells were grown in 96-well plates (10⁴ cells/well) and were exposed to different doses of NPs (from µg/mL) in serum-free MEM-F12-ITS medium for 24 h. For uptake experiments, the cells were grown in 24-well plates (10⁵ cells/well) and were exposed to 50 µg NPs (10¹⁰ NPs/mL) in MEM-F12-ITS medium for 1 h. During exposure to NPs, the cells were kept at 37 °C in a 5% CO₂ and 95% air atmosphere incubator. The NP dispersions were prepared immediately before use and vortexed before distribution in the culture wells.

Cell viability assays (MTT reduction)

For assessing MTT reduction, an index of cellular activity, we used the redox reaction of the same compound 3-(4,5-dimethylthiazol-2-yl)-2,5-diphenyltetrazolium bromide (MTT). MTT can be reduced to a purple formazan,^[42] and formazan production can be determined by photometrically measuring the absorption of light in the wavelength range of 550–570 nm. The metabolic activity of cells was measured by the MTT reduction assay on living cells.^[42]

Cells grown on 96-well plates (10⁴ cells/well) were exposed to NP suspensions (from 7.8 to 250 µg/mL) in 100 µL of MEM-F12-ITS. The cells were incubated for 24 h at 37 °C in 95% air and 5% CO₂ atmosphere. The reaction was stopped by adding 100 µL stop solution containing 50% dimethylformamide and 20% sodium dodecyl sulfate in distilled water (DMF-SDS, pH 4.7). After dissolving the cell material and the formazan product in the stop solution, formazan quantity was determined by measuring light absorption at dual [550–570 nm (measuring) and 630–650 nm (reference)] wavelengths using a Bio-Rad 450 (BioRad Hungary Ltd., Budapest, Hungary) or Dynatech MR5000 (Dynatech Industries Inc., McLean, VA). To obtain comparable data on different cells and culture plates, optical density data measured in each well were related to

values obtained on control (non-exposed) cells on the same plate (100%). The data were presented as relative percentages of the control. Averages and standard deviations were calculated from 8–12 identically treated cultures. Significance was calculated with the Student *t*-test. Differences were regarded statistically significant if *p*-values were < 0.05 and biologically significant if dose-dependent responses were detected.

TEM analysis of the cellular uptake of AgNPs of different shape

Neural stem cells were grown on poly-L-lysine-coated glass coverslips in 24 well plates (10⁵ cells/well). The cells were incubated with 500 µL suspension of 50 µg/mL (2×10¹¹ NPs/mL) NPs dispersed in MEM-F12-ITS for 1 h at 37 °C in a CO₂ incubator. Control cells were incubated without NPs. The cells were washed three times with PBS (pH 7.4) to remove free-floating NPs and fixed for 20 min with freshly prepared glutaraldehyde 1% and 4% PFA solution before being post fixed in 2% osmium tetroxide (OsO₄) in 0.1 M PBS pH 7.4 at 4 °C for 2 hours. After washing, the preparations were dehydrated in increasing (30%, 60%, 96% v/v) concentrations of ethanol and embedded in LX-112 resin (Ladd, Burlington, VT). Sections (60–80 nm) were cut with an ultracut (UCT, Leica EM UC7, Wetzlar, Germany) and then contrasted with 1% uranyl-acetate in 50% ethanol and examined by TEM as above.

Declarations

Funding This study was supported by the EU FP7 Marie Curie Actions, Network for Initial Training NanoTOES (PITN-GA-2010-264506). ICN2 is supported by the Severo Ochoa program from Spanish MINECO (grant no. SEV-2017-0706) and is funded by the CERCA Programme/Generalitat de Catalunya

Conflict of Interest

The authors declare no conflict of interest

Keywords: Silver nanoparticles · geometries · cellular uptake · neurotoxicity · neural stem cells · protein corona

- [1] M. E. Vance, T. Kuiken, E. P. Vejerano, S. P. McGinnis, M. F. Hochella, Jr., D. Rejeski, M. S. Hull, *Beilstein J. Nanotechnol.* **2015**, *6*, 1769–1780.
- [2] a) D. Morris, M. Ansar, J. Speshock, T. Ivanciuc, Y. Qu, A. Casola, R. Garofalo, *Viruses* **2019**, *11*, 732; b) T. Thi Ngoc Dung, V. Nang Nam, T. Thi Nhan, T. T. B. Ngoc, L. Q. Minh, B. T. T. Nga, V. Phan Le, D. Viet Quang, *Mater. Res. Express* **2020**, *6*, 1250–1259; c) X. X. Yang, C. M. Li, C. Z. Huang, *Nanoscale* **2016**, *8*, 3040–3048; d) M. B. Genter, N. C. Newman, H. G. Shertzer, S. F. Ali, B. Bolon, *Toxicol. Pathol.* **2012**, *40*, 1004–1013.
- [3] E. S. Patchin, D. S. Anderson, R. M. Silva, D. L. Uyeminami, G. M. Scott, T. Guo, L. S. Van Winkle, K. E. Pinkerton, *Environ. Health Perspect.* **2016**, *124*, 1870–1875.
- [4] a) G. J. Garcia, J. D. Schroeter, J. S. Kimbell, *Inhalation Toxicol.* **2015**, *27*, 394–403; b) T. Kovács, *Ageing Res. Rev.* **2004**, *3*, 215–232; c) L. Tian, Y. Shang, R. Chen, R. Bai, C. Chen, K. Inthavong, J. Tu, *Part. Fibre Toxicol.* **2019**, *16*, 1–17.
- [5] a) G. Oberdorster, A. Elder, A. Rinderknecht, *J. Nanosci. Nanotechnol.* **2009**, *9*, 4996–5007; b) G. Oberdorster, Z. Sharp, V. Atudorei, A. Elder, R. Gelein, W. Kreyling, C. Cox, *Inhalation Toxicol.* **2004**, *16*, 437–445; c) B. Wang, W. Y. Feng, M. Wang, J. W. Shi, F. Zhang, H. Ouyang, Y. L. Zhao, Z. F. Chai, Y. Y. Huang, Y. N. Xie, H. F. Wang, J. Wang, *Biol. Trace Elem. Res.* **2007**, *118*, 233–243.
- [6] L. Illum, *Eur. J. Pharm. Sci.* **2000**, *11*, 1–18.

- [7] a) M. Aschner, *Prog. Brain Res.* **2009**, *180*, 141–152; b) A. J. De Lorenzo, *Ann. Otol. Rhinol. Laryngol.* **1960**, *69*, 410–420; c) A. Elder, R. Gelein, V. Silva, T. Feikert, L. Opanashuk, J. Carter, R. Potter, A. Maynard, Y. Ito, J. Finkelstein, G. Oberdorster, *Environ. Health Perspect.* **2006**, *114*, 1172–1178; d) L. E. Hopkins, E. S. Patchin, P. L. Chiu, C. Brandenberger, S. Smiley-Jewell, K. E. Pinkerton, *Nanotoxicology* **2014**, *8*, 885–893; e) A. Mistry, S. Stolnik, L. Illum, *Int. J. Pharm.* **2009**, *379*, 146–157; f) S. Patel, S. Chavhan, H. Soni, A. K. Babbar, R. Mathur, A. K. Mishra, K. Sawant, *J. Drug Targeting* **2011**, *19*, 468–474.
- [8] a) M. Dan, H. Wen, A. Shao, L. Xu, *J. Biomed. Nanotechnol.* **2018**, *14*, 1330–1338; b) H. S. Sharma, S. F. Ali, S. M. Hussain, J. J. Schlager, A. Sharma, *J. Nanosci. Nanotechnol.* **2009**, *9*, 5055–5072.
- [9] K. Kalishwaralal, E. Banumathi, S. Ram Kumar Pandian, V. Deepak, J. Muniyandi, S. H. Eom, S. Gurunathan, *Colloids Surf. B* **2009**, *73*, 51–57.
- [10] W. J. Trickler, S. M. Lantz-McPeak, B. L. Robinson, M. G. Paule, W. Slikker, Jr., A. S. Biris, J. J. Schlager, S. M. Hussain, J. Kanungo, C. Gonzalez, S. F. Ali, *Drug Metab. Rev.* **2014**, *46*, 224–231.
- [11] J. H. Shannahan, R. Podila, A. A. Aldossari, H. Emerson, B. A. Powell, P. C. Ke, A. M. Rao, J. M. Brown, *Toxicol. Sci.* **2015**, *143*, 136–146.
- [12] a) V. De Matteis, M. A. Malvindi, A. Galeone, V. Brunetti, E. De Luca, S. Kote, P. Kshirsagar, S. Sabella, G. Bardi, P. P. Pompa, *Nanomedicine* **2015**, *11*, 731–739; b) L. C. Stoehr, E. Gonzalez, A. Stampfl, E. Casals, A. Duschl, V. Puentes, G. J. Oostingh, *Part. Fibre Toxicol.* **2011**, *8*, 1–15.
- [13] a) P. V. Asharani, M. P. Hande, S. Valiyaveetil, *BMC Cell Biol.* **2009**, *10*, 65; b) K. Urbanska, B. Pajak, A. Orzechowska, J. Sokolowska, M. Grodzik, E. Sawosz, M. Szmjdt, P. Sysa, *Nanoscale Res. Lett.* **2015**, *10*, 98.
- [14] E. M. Luther, Y. Koehler, J. Diendorf, M. Epple, R. Dringen, *Nanotechnology* **2011**, *22*, 375101.
- [15] E. Soderstjerna, F. Johansson, B. Klefbohm, U. Englund Johansson, *PLoS One* **2013**, *8*, e58211.
- [16] a) F. Xu, C. Pieltt, S. Farkas, M. Qazzaz, N. I. Syed, *Mol. Brain Res.* **2013**, *6*, 1–15; b) N. Repar, H. Li, J. S. Aguilar, Q. Q. Li, D. Drobne, Y. Hong, *Nanotoxicology* **2018**, *12*, 104–116.
- [17] R. Madathiparambil Visalakshan, L. E. Gonzalez Garcia, M. R. Benziger, A. Ghazaryan, J. Simon, A. Mierczynska-Vasilev, T. D. Michl, A. Vinu, V. Mailander, S. Morsbach, K. Landfester, K. Vasilev, *Small* **2020**, *16*, e2000285.
- [18] E. C. Cho, L. Au, Q. Zhang, Y. Xia, *Small (Weinheim an der Bergstrasse, Germany)* **2010**, *6*, 517–522.
- [19] a) M. Kumarasamy, A. Sosnik, *Adv. Biosyst.* **2019**, *3*, 1900123; b) K. Murali, K. Kenesei, Y. Li, K. Demeter, Z. Környei, E. Madarász, *Nanoscale* **2015**, *7*, 4199–4210; c) E. Izak-Nau, K. Kenesei, K. Murali, M. Voetz, S. Eiden, V. F. Puentes, A. Duschl, E. Madarasz, *Nanotoxicology* **2014**, *8*, 138–148.
- [20] a) M. Kumarasamy, A. Sosnik, *bioRxiv* **2020**; b) M. Kumarasamy, A. Sosnik, *iScience* **2021**, *24*, 102183.
- [21] a) X. Qi, T. Balankura, Y. Zhou, K. A. Fichthorn, *Nano Lett.* **2015**, *15*, 7711–7717; b) I. A. Safo, M. Werheid, C. Dosche, M. Oezaslan, *Nanoscale Adv.* **2019**, *1*, 3095–3106; c) Y. J. Song, M. Wang, X. Y. Zhang, J. Y. Wu, T. Zhang, *Nanoscale Res. Lett.* **2014**, *9*, 17; d) J. Patarroyo, A. Genç, J. Arbiol, N. G. Bastús, V. Puentes, *Chem. Commun.* **2016**, *52*, 10960–10963.
- [22] a) Y. Sun, Y. Xia, *Science* **2002**, *298*, 2176–2179; b) B. Wiley, Y. Sun, B. Mayers, Y. Xia, *Chemistry (Easton)* **2005**, *11*, 454–463.
- [23] I. Khan, K. Saeed, I. Khan, *Arab. J. Chem.* **2019**, *12*, 908–931.
- [24] C. S. S. R. Kumar, H. Jing, *UV-VIS and photoluminescence spectroscopy for nanomaterials characterization*, Springer Reference, Berlin; New York, **2013**.
- [25] Q. Zhang, W. Li, L.-P. Wen, J. Chen, Y. Xia, *Chemistry* **2010**, *16*, 10234–10239.
- [26] M. A. Raza, Z. Kanwal, A. Rauf, A. N. Sabri, S. Riaz, S. Naseem, *Nanomaterials* **2016**, *6*, 74.
- [27] a) C. Li, L. Sun, Y. Sun, T. Teranishi, *Chem. Mater.* **2013**, *25*, 2580–2590; b) Y. Sun, B. Gates, B. Mayers, Y. Xia, *Nano Lett.* **2002**, *2*, 165–168; c) Y. Sun, Y. Xia, *Adv. Mater. (Weinheim, Ger.)* **2002**, *14*, 833–837; d) Y. Sun, B. Mayers, T. Herricks, Y. Xia, *Nano Lett.* **2003**, *3*, 955–960.
- [28] L. Vroman, A. L. Adams, G. C. Fischer, P. C. Munoz, *Blood* **1980**, *55*, 156–159.
- [29] J. E. Gagner, M. D. Lopez, J. S. Dordick, R. W. Siegel, *Biomaterials* **2011**, *32*, 7241–7252.
- [30] Z. Ferdous, A. Nemmar, *Int. J. Mol. Sci.* **2020**, *21*, 2375.
- [31] J. G. Teeguarden, P. M. Hinderliter, G. Orr, B. D. Thrall, J. G. Pounds, *Toxicol. Sci.* **2007**, *95*, 300–312.
- [32] a) A. Balfourier, N. Luciani, G. Wang, G. Lelong, O. Ersen, A. Khelfa, D. Alloyeau, F. Gazeau, F. Carn, *Proc. Natl. Acad. Sci. USA* **2020**, *117*, 103–113; b) A. Espinosa, A. Curcio, S. Cabana, G. Radtke, M. Bugnet, J. Kolosnjaj-Tabi, C. Péchoux, C. Alvarez-Lorenzo, G. A. Botton, A. K. A. Silva, A. Abou-Hassan, C. Wilhelm, *ACS Nano* **2018**, *12*, 6523–6535.
- [33] J. Jiang, G. Oberdörster, A. Elder, R. Gelein, P. Mercer, P. Biswas, *Nanotoxicology* **2008**, *2*, 33–42.
- [34] a) Y. He, K. Park, *Mol. Pharm.* **2016**, *13*, 2164–2171; b) V. Forest, L. Leclerc, J. F. Hocheplid, A. Trouvé, G. Sarry, J. Pourchez, *Toxicol. in Vitro* **2017**, *38*, 136–141; c) C. Huang, Y. Zhang, H. Yuan, H. Gao, S. Zhang, *Nano Lett.* **2013**, *13*, 4546–4550; d) J. H. Lee, J. E. Ju, B. I. Kim, P. J. Pak, E. K. Choi, H. S. Lee, N. Chung, *Environ. Toxicol. Chem.* **2014**, *33*, 2759–2766; e) N. Oh, J. H. Park, *Int. J. Nanomed.* **2014**, *9* Suppl 1, 51–63; f) S. Salatin, S. Maleki Dizaj, A. Yari Khosroushahi, *Cell Biol. Int.* **2015**, *39*, 881–890; g) X. Xie, J. Liao, X. Shao, Q. Li, Y. Lin, *Sci. Rep.* **2017**, *7*, 3827.
- [35] a) L. Dong, S. Tang, F. Deng, Y. Gong, K. Zhao, J. Zhou, D. Liang, J. Fang, M. Hecker, J. P. Giesy, X. Bai, H. Zhang, *Sci. Total Environ.* **2019**, *690*, 158–166; b) M. Allegri, M. G. Bianchi, M. Chiu, J. Varet, A. L. Costa, S. Ortelli, M. Blosi, O. Bussolati, C. A. Poland, E. Bergamaschi, *PLoS One* **2016**, *11*, e0151365.
- [36] J. N. Smith, D. G. Thomas, H. Jolley, V. K. Kodali, M. H. Littke, P. Munusamy, D. R. Baer, M. J. Gaffrey, B. D. Thrall, J. G. Teeguarden, *Part. Fibre Toxicol.* **2018**, *15*, 47.
- [37] N. G. Bastús, F. Merkoçi, J. Piella, V. Puentes, *Chem. Mater.* **2014**, *26*, 2836–2846.
- [38] Q. Zhang, N. Li, J. Goebel, Z. Lu, Y. Yin, *J. Am. Chem. Soc.* **2011**, *133*, 18931–18939.
- [39] J. Ma, M. Zhan, *RSC Adv.* **2014**, *4*, 21060–21071.
- [40] A. J. Rai, C. A. Gelfand, B. C. Haywood, D. J. Warunek, J. Yi, M. D. Schuchard, R. J. Mehig, S. L. Cockrill, G. B. Scott, H. Tammen, P. Schulz-Knappe, D. W. Speicher, F. Vitzthum, B. B. Haab, G. Siest, D. W. Chan, *Proteomics* **2005**, *5*, 3262–3277.
- [41] K. Schlett, E. Madarasz, *J. Neurosci. Res.* **1997**, *47*, 405–415.
- [42] T. Mosmann, *J. Immunol. Methods* **1983**, *65*, 55–63.

Submitted: May 17, 2022

Accepted: September 23, 2022